# Poliovirus evolution towards independence from the phosphatidylinositol-4 kinase III $\beta$/oxysterol-binding protein family I pathway

Minetaro Arita, Joelle Bigay

# Poliovirus evolution towards independence from the phosphatidylinositol-4 kinase III β/oxysterol-binding protein family I pathway

Minetaro Arita[1*] and Joëlle Bigay[2]

[1]Department of Virology II, National Institute of Infectious Diseases, 4-7-1 Gakuen, Musashimurayama-shi, Tokyo 208-0011, Japan

[2]Université Côte d'Azur, CNRS, Institut de Pharmacologie Moléculaire et Cellulaire, 660 route des lucioles, 06560 Valbonne, France

*To whom correspondence should be addressed:
Department of Virology II, National Institute of Infectious Diseases,
4-7-1 Gakuen, Musashimurayama-shi, Tokyo 208-0011, Japan
Phone:+81-42-561-0771; Fax:+81-42-561-4729
e-mail: minetaro@nih.go.jp

**Abstract**

Phosphatidylinositol-4 kinase III β (PI4KB) and oxysterol-binding protein (OSBP) family I provide a conserved host pathway required for enterovirus replication. Here, we analyze the role and essentiality of this pathway in enterovirus replication. Phosphatidylinositol 4-phosphate (PI4P) production and cholesterol accumulation in the replication organelle (RO) are severely suppressed in cells infected with a poliovirus (PV) mutant isolated from a *PI4KB*-knockout cell line (RD[Δ*PI4KB*]). Major determinants of the mutant for infectivity in RD(Δ*PI4KB*) cells map to the A5270U(3A-R54W) and U3881C(2B-F17) mutations. The 3A mutation is required for PI4KB-independent development of RO. The 2B mutation rather sensitizes PV to PI4KB/OSBP inhibitors by itself, but confers substantially complete resistance to the inhibitors with the 3A mutation, suggesting that the PI4KB/OSBP pathway is not necessarily essential for enterovirus replication *in vitro*. This work supports a two-step resistance model of enterovirus, and offers insights into a potential evolutionary pathway of enterovirus towards independence from the PI4KB/OSBP pathway.

Keywords: virus / picornavirus / enterovirus / PI4KB / OSBP / resistance

For Table of Contents Use Only

Title: Poliovirus evolution towards independence from the phosphatidylinositol-4 kinase III β / oxysterol binding protein family I pathway

Author: Minetaro Arita and Joëlle Bigay

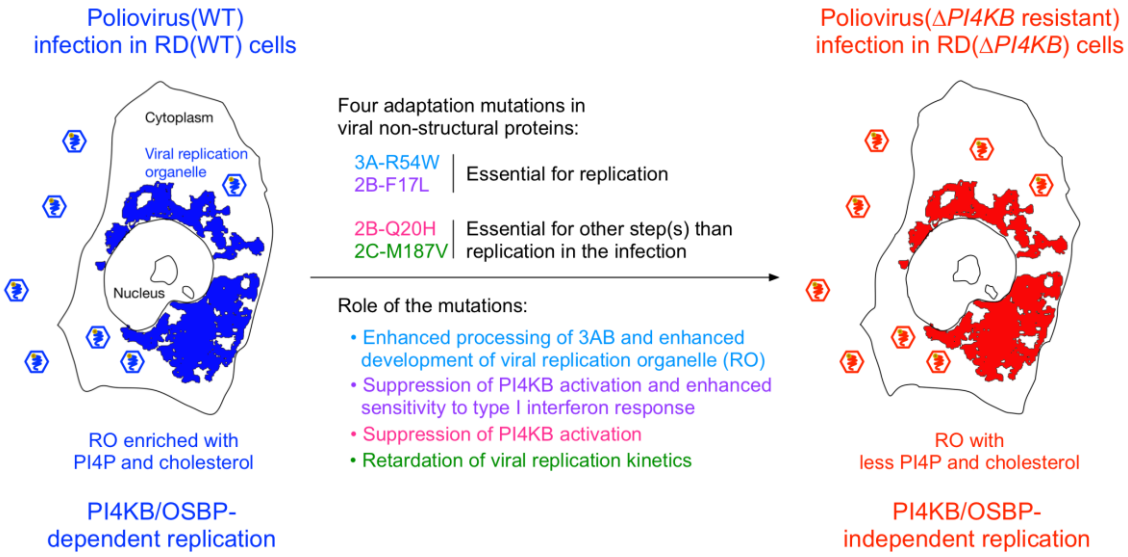


**Poliovirus evolution towards PI4KB/OSBP-independent infection**

## Introduction

Poliovirus (PV) is a small non-enveloped virus with a positive-sense single-stranded RNA genome of about 7500 nt belonging to the genus *Enterovirus*, in the family *Picornaviridae*. PV causes poliomyelitis by destroying motor neurons [1,2]. In the global PV eradication program initiated in 1988, antivirals against PV were anticipated to have important roles to play in both the endgame and the post-eradication era. However, no antivirals are currently available for PV infection.

Among the many host factors identified for PV replication, Phosphatidylinositol-4 kinase III β (PI4KB) and oxysterol-binding protein (OSBP) have been considered as the potential targets of antiviral for enterovirus based on the effectiveness of the identified inhibitors and on the conserved role in enterovirus replication [3-13]. The importance of PI4KB in enterovirus replication was originally recognized by Hsu *et al*. [14], with a potent PI4KB inhibitor PIK93 [15]. PI4KB is one of the four mammalian PI4 kinases (PI4K2A, PI4K2B, PI4KA, and PI4KB) [16]. PI4KB produces PI4P mainly at the Golgi, and is involved in membrane trafficking from the Golgi. Oxysterol-binding protein (OSBP) family I was then identified as the target of a minor group of enviroxime-like compounds [11,12,17]. OSBP transfers cholesterol between endoplasmic reticulum and *trans* Golgi in a phosphatidylinositol 4-phosphate (PI4P)-dependent manner, and contributes to the homeostasis of cholesterol and lipid [18-21]. Functional links between PI4KB and OSBP family I in PV replication were originally suggested by a conserved resistance mutation in 3A protein to PI4KB/OSBP inhibitors [8,22]. PI4KB activated by the viral proteins (2C, 2BC, 3AB, 3CD, and 3D)

provides PI4P for recruitment of OSBP, then OSBP accumulates cholesterol at the replication organelle (RO) to facilitate the cleavage of 3AB and the formation of viral replication complex for the synthesis of viral plus-strand RNA [4,12,22-28]. The PI4KB/OSBP pathway is conserved in the replication of Aichivirus, which belongs to another genus in the family *Picornaviridae* (genus *Kobuvirus*) [29]. A similar pathway is conserved in the replication of encephalomyocarditis virus (EMCV) (genus *Cardiovirus* in the family *Picornaviridae*) or hepatitis C virus (family *Flaviviridae*), where PI4KA and in part PI4KB act for the recruitment of OSBP [30-36].

Despite the conservation of the PI4KA,B/OSBP pathway requirement in the replication of a broad range of picornaviruses, replication of viruses in the genus *Aphthovirus* does not depend on the PI4KA,B/OSBP pathway [12,37,38]. This raised a question about the essentiality of the PI4KB/OSBP pathway in enterovirus replication. Here, we investigate the role and essentiality of the PI4KB/OSBP pathway in enterovirus replication. We isolated a PV mutant that showed substantially complete resistance to PI4KB/OSBP inhibitors, and characterized the mechanism of resistance. In addition, we provide a model of PV evolution towards independence from the PI4KB/OSBP pathway.

## Results and Discussion

**Generation of *PI4KB*-knockout cell line.** To characterize viral replication independent of the PI4KB/OSBP pathway, we generated a *PI4KB*-knockout cell line (RD[Δ*PI4KB*]) highly resistant to PV infection using a CRISPR/Cas9 system (**Figure 1**). *PI4KB* alleles of RD(Δ*PI4KB*) cells showed 1-nt insertion or 26-nt deletion and caused termination after aa 351 or 348 of PI4KB (**Figure 1A**). Expression of full-length PI4KB was not detected in RD(Δ*PI4KB*) cells, in contrast to parental RD(WT) cells that showed two bands of PI4KB corresponding to a 4,260-Da modification [13] (**Figure 1B**). To analyze potential off-target effects of the CRISPR/Cas9 system, we performed *trans* rescue of PV replication with ectopic expression of PI4KB (**Figure 1C**). Expression of PI4KB(WT), but not of a kinase-dead PI4KB(D656A) mutant, rescued $PV1_{pv}$ infection in RD(Δ*PI4KB*) cells, and its effects was suppressed by MDL-860, an allosteric PI4KB inhibitor [13]. Moreover, *trans* rescue with the PI4KB(C646S) mutant, which is resistant to covalent modification/inactivation by MDL-860 [13], showed no suppression of $PV1_{pv}$ infection by MDL-860, suggesting that PI4KB provided in *trans* supports PV replication in RD(Δ*PI4KB*) cells. $PV1_{pv}$ infection was suppressed more than 10,000-fold in RD(Δ*PI4KB*) cells compared to RD(WT) cells, corresponding to treatment with >40 μM of the PI4KB inhibitor T-00127-HEV1 [25]. In contrast, the susceptibility of RD(Δ*PI4KB*) to infection by Sendai virus (family *Paramyxoviridae*), which is resistant to PI4KB inhibitor [6], was similar to that of RD(WT) cells (**Figure 1D**). These results suggested that PV replication in RD(Δ*PI4KB*) cells was suppressed by specific depletion of active PI4KB, but not by other potential off-target effects of the

CRISPR/Cas9 system.

**Isolation of PV mutant from RD(Δ*PI4KB*) cells.** To clarify the essentiality of the PI4KB/OSBP pathway in PV replication, we attempted to isolate PV mutant from RD(Δ*PI4KB*) cells (**Table 1**). Infectivity of parental PV1(Sabin) in RD(Δ*PI4KB*) cells was reduced more than 100,000-fold compared to RD(WT) cells. After nine rounds of passage of PV1(Sabin) in RD(Δ*PI4KB*) cells, we isolated a PV mutant (PV[Δ*PI4KB* resistant], clone 1) that could efficiently replicate in RD(Δ*PI4KB*) cells as efficiently as EMCV.

PV(Δ*PI4KB* resistant) contained one mutation in the non-coding region, three synonymous mutation, and six non-synonymous mutations (**Figure 2A**). We focused on the analysis of non-synonymous mutations, because observed synonymous mutations are not apparently associated with *cis* elements in PV genome. To clarify the evolutionary link between mutations, we analyzed genomic sequences and the infectivity of PV (pooled population) obtained after each passage in RD(Δ*PI4KB*) cells and an additional virus isolate (clone 2) obtained after nine passages (**Supplementary Figure1**). We observed sequential fixation of 3A-R54W, 2B-F17L, 2C-M187V and 2B-Q20H mutations. The 2C-M187V mutation appeared as early as the second passage, but required an additional two passages to become fixed in the population. Infectivity of the viral population in RD(Δ*PI4KB*) cells correlated with fixation of the four mutations. Genomic sequencing of additional PV isolate after nine passages (clone 2), confirmed fixation of these four non-synonymous mutations, suggesting that the 2A-F80L and 3A-E53D mutations of PV(Δ*PI4KB* resistant) play minor roles in the infectivity.

To determine the mutations required for infectivity in RD(Δ*PI4KB*) cells, a series of PV mutants was analyzed (**Figure 2B and Supplementary Figure 2**). $PV1_{pv}$ mutant ($PV1_{pv}$[Δ*PI4KB* resistant]), which has all the observed non-synonymous mutations of PV(Δ*PI4KB* resistant), showed drastically delayed replication kinetics in RD(WT) cells compared to $PV1_{pv}$(WT) (delay of about 6 h before plateauing) (**Supplementary Figure 1**). The major determinant of the delayed replication kinetics was the 2C-M187V mutation. $PV1_{pv}$ mutants without the 2C mutation still showed a delay in replication of about 2 h, which was similar to that of $PV1_{pv}$(139[+25aa]), which has reduced viral protein synthesis (17% of WT)[39]. Basal infectivity was slightly enhanced by the 2A mutation (210% of WT), but decreased by the 2B, 2C, and 3A mutations (64%, 63%, and 73% of WT, respectively).

We analyzed the effect of each mutation on the infectivity in RD(Δ*PI4KB*) cells. Reversion of the 2A and 2C mutations did not affect infectivity, while reversion in the 2B and 3A regions (2B-F17L and 3A-R54W mutations) significantly decreased infectivity (**Figure 2B**), suggesting that these two mutations act as the major determinants of infectivity (mutants 1, 2, 3, 4, and 5). The aa 54 of the 3A protein has been reported for other enterovirus mutants resistant to PI4KB/OSBP inhibitors [40 7 41]. The 3A mutations increased infectivity in RD(Δ*PI4KB*) cells 290- to 2,400-fold (mutant 9), with a major influence of the 3A-R54W mutation (mutants 4 and 5). The mutations in 2A, 2B, and 2C did not enhance infectivity by themselves (mutants 6,7, and 8). The 2B-Q20H, 2C-M187V, and 3A-E53D mutations showed minor but significant contributions with the 3A-R54W mutation to infectivity (about 2-fold increase at 7 h p.i.), although the effect of the 2A mutation was not significant in the presence of the

2B and 3A mutations (mutants 10, 11, and 12). This suggests that 2C-M187V and 2B-Q20H mutations have major role in some other step(s) in infection than replication to enhance the infectivity in RD(Δ*PI4KB*) cells (**Supplementary Figure 1**). Introduction of 2B-F17L and 3A-R54W mutations could confer a similar level of infectivity to that of $PV1_{pv}$[Δ*PI4KB* resistant] (mutant 13). $PV1_{pv}$(139[+25aa]) did not show any infectivity similar to $PV1_{pv}$(WT), suggesting that delayed replication kinetics are not the determinant for infectivity in RD(Δ*PI4KB*) cells. Among the mutants examined, the highest infectivity was observed for a $PV1_{pv}$ mutant that had all the mutations of $PV1_{pv}$[Δ*PI4KB* resistant] except the 2C mutation (mutant $PV1_{pv}$[Δ*PI4KB* resistant [-2C]]). All these results suggested that the 3A-R54W mutation acts as the major primary determinant, which is the essential prerequisite for infectivity in RD(Δ*PI4KB*) cells, and that the 2B-F17L mutation is the major synthetic determinant, and enhances the infectivity conferred by the 3A mutation.

**Roles of mutations in PI4KB-independent replication.** The target of PI4KB/OSBP inhibitors is in the formation of viral replication complex on RO [4]. We therefore analyzed the effects of mutations in PV(Δ*PI4KB* resistant) on the development of RO in RD(Δ*PI4KB*) cells (**Figure 3**). As a marker of the RO, on which the active viral replication complex is formed [42], we used 2B protein that co-localizes with viral nascent RNA and PI4KB on the surface area of the RO (**Supplementary Figure 3**). Because $PV1_{pv}$(WT) could not replicate in RD(Δ*PI4KB*) cells, we analyzed RO development in a replication-incompetent system by ectopic expression of a viral polyprotein precursor N-terminally fused with EGFP (EGFP-2BC3ABCD). RO development by

EGFP-2BC3ABCD(WT) was severely suppressed in RD(Δ*PI4KB*) cells resulting in the development of small RO. Introduction of 3A mutations (E53D and R54W) to EGFP-2BC3ABCD, but not of the 2B mutations, restored the population of RD(Δ*PI4KB*) cells with a normal-sized RO. Addition of the 2B mutations to the 3A mutant did not further increase the population of cells with normal-sized RO. We also analyzed the effects of the G5318A(3A-A70T) mutation, which confers a partial resistance to PI4KB/OSBP inhibitors [22,25], on RO development. Interestingly, the 3A-A70T mutation did not restore the size of the RO in RD(Δ*PI4KB*) cells in contrast to the 3A mutations (**Supplementary Figure 4**). The 3A mutations (E53D and R54W) conferred higher infectivity than the 3A-A70T mutation (**Supplementary Figure 5**), suggesting a correlation between RO development and infectivity in RD(Δ*PI4KB*) cells. The synthetic effects of 2B mutations on the infectivity were similarly observed with these 3A mutations (**Supplementary Figure 5**). These results suggested that the 3A mutations of PV(Δ*PI4KB* resistant), but not the 2B mutations, are essential for the development of RO in PI4KB-independent replication, and that the synthetic effect of the 2B mutations is independent of the 3A mutations.

Next, we analyzed the effects of 3A mutations on the processing of 3AB, which is enhanced in enteroviruses that are partially resistant to PI4KB inhibitor [25,26]. The 3A mutations (E53D and R54W) enhanced processing of 3AB as well as the 3A-A70T mutation in infected cells (**Supplementary Figure 6A**). The 2B mutations caused apparent suppression of the 3AB processing at 9 h p.i. compared to that of WT, but similar suppression to that of WT at 7 h p.i., suggesting that the effect was attributable to the delayed replication kinetics conferred by 2B mutations. Introduction

of 3A mutations to the 2B mutant restored the processing of 3AB. We also attempted to analyze 3AB processing in a replication-incompetent system (processing of EGFP-2BC3ABCD). The 2B, 2BC, 3D, and 3CD were clearly detected as observed in the infected cells, but the 3A was barely detectable and the 3AB was not detected (**Supplementary Figure 6B**). This suggested that the 3A mutations of PV(Δ*PI4KB* resistant), but not the 2B mutations, contribute to the enhanced processing of 3AB.

We analyzed the effect of 2B mutations on the replication level of PV in a single cell (**Figure 4**). $PV1_{pv}$(WT)-infected RD(WT) cells showed about 1,000 and 1,200 RLU of luciferase signals per cell at 7 and 16 h p.i., respectively. $PV1_{pv}$ mutants showed similar replication levels to those of $PV1_{pv}$(WT) in RD(WT) cells. RD(Δ*PI4KB*) cells infected with the 3A mutant showed about 400 and 500 RLU per infected cell at 7 and 16 h p.i., respectively. The 2B mutations enhanced replication levels about 2-fold (700 and 900 RLU per infected cell at 7 and 16 h p.i., respectively). Addition of the 2A mutation ($PV1_{pv}$(Δ*PI4KB* resistant [-2C]) mutant) increased levels by about 2 fold at 16 h p.i. (1,700 RLU per infected cell), but not at 7 h p.i. (800 RLU per infected cell). This suggests that enhancement of early-stage replication by 2B mutation is essential for PI4KB-independent replication.

**The 2B mutations suppressed activation of PI4KB.** To further characterize the role of PV(Δ*PI4KB* resistant) mutations, we analyzed levels of PI4P and cholesterol in RD(WT) and RD(Δ*PI4KB*) cells infected with $PV1_{pv}$(Δ*PI4KB* resistant [-2C]) (**Figure 5 and Supplementary Figure 7**). In contrast to $PV1_{pv}$(WT) infection, $PV1_{pv}$(Δ*PI4KB* resistant [-2C]) infection caused a minimum enhancement of PI4P level (about 1.1-fold

enhancement at 7 h p.i.), dot-like localization of PI4P in the cells, and reduced accumulation of cholesterol in the RO in favor of the plasma membrane. In $PV1_{pv}$(Δ*PI4KB* resistant [-2C])-infected RD(Δ*PI4KB*) cells (about 0.5-1.0% of total population at 7 h p.i.), PI4P levels decreased somewhat (about a 0.84-fold change at 7 h p.i.), and no accumulation of PI4P/cholesterol in the RO was observed (**Supplementary Figure 8**). To identify determinants for the suppressed PI4KB activation in RD(WT) cells, we quantified PI4P levels infected with $PV1_{pv}$ mutants (**Figure 6A**). $PV1_{pv}$(139[+25aa]) infection, which was used as a control with delayed replication kinetics, rather enhanced the PI4P levels. The 2B-F17L mutation reduced PI4P levels to about 60% of that in $PV1_{pv}$(WT)-infected cells, indicating that the mutation acts as a major determinant for the suppression of PI4P production. $PV1_{pv}$(Δ*PI4KB* resistant [-2C]) suppressed PI4P levels more severely (about 30% of $PV1_{pv}$(WT)-infected cells, and 20% of $PV1_{pv}$(139[+25aa])-infected cells), suggesting the existence of other determinants. We further analyzed the PI4P levels of infected cells with other $PV1_{pv}$ mutants, and identified the 2B-Q20H mutation as another major determinant (**Figure 6B**). Removal of either 2B-F17L or 2B-Q20H mutation (mutants 3 and 2, respectively) restored PI4P levels, and introduction of these mutations (mutant 7) caused the highest suppression of PI4P levels. The 2C and 3A mutations could not further enhance suppression of PI4P levels caused by the 2B mutations. These results suggest that $PV1_{pv}$(Δ*PI4KB* resistant [-2C]) could replicate without overproduction of PI4P, and sequential adaptation of PV to an altered lipid environment with less PI4P and cholesterol with the 2B mutations.

**Complete resistance of PV mutant to PI4KB/OSBP inhibitors.** We analyzed sensitivity of PV(Δ*PI4KB* resistant) to PI4KB/OSBP inhibitors (**Figure 7**). We used T-00127-HEV1 as a specific PI4KB inhibitor, and T-00127-HEV2 as an OSBP inhibitor targeting sterol transfer. T-00127-HEV2 inhibited sterol-transfer activity of OSBP as well as other OSBP inhibitors (25-HC and itraconazole), but had a lower effect on PI4P transfer, suggesting that T-00127-HEV2 acts as a 25-HC-like sterol competitor on OSBP (**Supplementary Figure 9**) [12,18,43]. $PV1_{pv}$ mutants with the 2B and 3A mutations showed substantial resistance to PI4KB/OSBP inhibitors even at a high concentration (40 μM), in contrast to a $PV1_{pv}$ mutant with the 3A-A70T mutation ($PV1_{pv}$[enviroxime resistant]), which is only partially resistant to PI4KB/OSBP inhibitors [25](**Figure 7A**). This further supports the notion that PI4KB and OSBP are part of the inseparable functional axis in enterovirus replication [12,24], and indicates that the PI4KB/OSBP pathway is not necessarily essential for the replication of enterovirus *in vitro*. OSBP could use PI4P from PI4Ks (particularly PI4K2A) other than PI4KB [43]. Observed resistance to OSBP inhibitor suggested that alternative activation of other PI4Ks are not essential for the resistance.

Infection of $PV1_{pv}$(Δ*PI4KB* resistant [-2C]) in RD(WT) cells could be suppressed to about 20% at high concentrations of PI4KB inhibitor, suggesting that about 80% of $PV1_{pv}$(Δ*PI4KB* resistant [-2C]) replication still depends on the PI4KB/OSBP pathway in RD(WT) cells. The 3A mutations conferred higher resistance to PI4KB inhibitor than the 3A-A70T mutation at high concentrations, but not at low concentrations. Interestingly, the 2B mutation rather sensitized PV to PI4KB/OSBP inhibitors, but conferred resistance to OSBP inhibitor at high concentration. These

results suggested a two-step resistance model of PV to PI4KB/OSBP inhibitors in which the 3A mutation acts as the primary resistance mutation by enhancing the processing of 3AB and the development of RO. The 3A mutation thus acts as a compensatory mutation to the 2B mutation that rather sensitizing PV to PI4KB/OSBP inhibitors by suppressive effects on PI4P production. The 2B mutation raises the replication level, possibly by enhancing the formation of viral replication complex on the RO (synthetic resistance) in the altered lipid environment by PI4KB/OSBP inhibitors. Thus, the 2B mutation could in turn act as a resistance mutation at high concentrations of PI4KB/OSBP inhibitors.

We attempted to determine the target viral proteins of the 3A and 2B mutations by *trans* complementation assay with virus proteins (**Supplementary Figure 10**). Overexpression of 3A/3AB could confer partial resistance to PI4KB inhibitor, as reported previously [25], but could not confer any resistance at high concentrations of inhibitor. We did not see any *trans* rescue effects with 2B/2BC proteins. These results suggest that modulation of the processing/overexpression of viral proteins is not the target of the mutations for the substantially complete resistance to PI4KB inhibitor.

Next, we analyzed the effects of PI4KB/OSBP inhibitors on PI4KB/OSBP-independent replication of PV (**Figure 7B**). OSBP inhibitor drastically enhanced the infection of $PV1_{pv}$(Δ*PI4KB* resistant [-2C]) in RD(Δ*PI4KB*) cells (>600% infection at 40 μM), in contrast to PI4KB inhibitor that showed substantially no suppression (>80% and >30% infection at 10 and 40 μM, respectively). To characterize the mechanisms underlying the observed adaptation to OSBP inhibitor, we analyzed the effects of other OSBP inhibitors (25-HC and itraconazole) on the replication of $PV1_{pv}$ with the 2B mutations (**Supplementary Figure 11**). We found that the 2B mutations

sensitized PV to itraconzole, but did not confer resistance to itraconazole at high concentrations, in contrast to T-00127-HEV2 and 25-HC (**Supplementary Figure 11A**). The 2B-F17L mutation acted as the major determinant for these phenotypes. T-00127-HEV2 and 25-HC, but not itraconazole, enhanced the replication of $PV1_{pv}$(Δ*PI4KB* resistant [-2C]) in RD(Δ*PI4KB*) cells (**Supplementary Figure 11B**). This suggested that the 2B mutation confers adaptation to the altered lipid environment formed by the 25-HC-like activity (low inhibitory effect on the PI4P-transfer activity of OSBP) or sterol-like chemical properties of OSBP inhibitors. Collectively, these results indicate that PV(Δ*PI4KB* resistant) could replicate independently of the PI4KB/OSBP pathway supported by the 3A and 2B mutations.

**Role of PI4KB/OSBP pathway in innate immune response.** To define potential biological roles of PI4KB/OSBP-independent PV replication, we analyzed the effect of type I interferon (IFN) response, which is a target of 2B and controls the tissue tropism of PV *in vivo* [44,45]. Pre-treatment of RD(WT) cells with IFN alpha suppressed $PV1_{pv}$(WT) infection (25% of mock treatment) (**Figure 8**). Interestingly, $PV1_{pv}$(Δ*PI4KB* resistant) infection was severely suppressed by the treatment in RD(WT) cells and RD(Δ*PI4KB*) cells (2.0% and 4.1% of mock treatment, respectively). Analysis of $PV1_{pv}$ mutants suggested the 2B-F17L mutation as the major determinant for sensitivity to IFN alpha; deletion of the mutation restored resistance (mutant 3), and addition of the mutation conferred sensitization to IFN alpha treatment. The 2C and 3A mutations conferred slight sensitization (mutants 8, 9, and 13). In contrast, the 2A mutation had no effect, and the 2B-Q20H mutation instead conferred weak resistance.

These results suggested that the PI4KB/OSBP pathway plays an important role in counteracting type I IFN response during PV replication. Mutations in 2B could suppress innate immune response in PV infection [45]. We found that replication of $PV1_{pv}$(Δ*PI4KB* resistant [-2C]) is hypersensitive to IFN alpha treatment, and that the 2B-F17L mutation acts as the major determinant for this sensitivity. Viktorova et al. recently showed the importance of choline/phosphatidylcholine in multiple cycles of PV infection to antagonize antiviral effects of type I IFN [46], suggesting a relationship between lipid composition of the RO and sensitivity to IFN. Our results suggest an evolutionary link between the PI4KB/OSBP pathway and innate immune response in enterovirus replication.

In summary, we characterized a PV mutant that shows substantially complete resistance to PI4KB/OSBP inhibitors, and found that the mutant acquired the resistance by a two-step mechanism involving unique epistatic interaction of the 3A and 2B mutations. This work offers novel insights into a potential evolutionary pathway of enterovirus towards independence from the PI4KB/OSBP pathway and may contribute to our fundamental understanding of the role of host factors and of strategies to overcome the viral resistance conferred by host-targeting antivirals.

## Methods

**Cells.** RD cells (human rhabdomyosarcoma cell line) and HEK293 cells (human embryonic kidney cells) were cultured as monolayers in Dulbecco's modified Eagle medium (DMEM) supplemented with 10% fetal calf serum (FCS). A *PI4KB*-knockout RD cell line was generated using a Clustered Regularly Interspaced Short Palindromic Repeats (CRISPR)/Cas9 GeCKO v2.0 system (a gift from Feng Zhang, Addgene, 1000000048)[47]. RD cells were transfected with a lentiCRISPRv2 plasmid encoding a targeting sequence for *PI4KB* gene (5'-ATAAGCTCCCTGCCCGAGTC-3') in the single-guide-RNA-coding region using a lipofectamine 3000 reagent (Invitrogen). A *PI4KB*-knockout cell line (RD[Δ*PI4KB*]) was obtained by subcloning of the transfected cells after selection with PV1(Sabin) infection.

**Viruses.** PV1(Sabin) is derived from a stock in NIID. Encephalomyocarditis virus (EMCV) was a kind gift from Kazuya Shirato (Department of Virology III, National Institute of Infectious Diseases, Japan). Luciferase-encoding Sendai virus (SeV-luc) was a kind gift from Atsushi Kato (Division of Quality Assurance, National Institute of Infectious Diseases, Japan). Wild-type type 1 PV pseudovirus ($PV1_{pv}$[WT]), which encapsidated luciferase-encoding PV replicon with the capsid protein of Mahoney strain, was used for evaluating infectivity. The G5318A(3A-A70T) mutation (enviroxime resistant) and newly identified mutations were introduced to $PV1_{pv}$. A $PV1_{pv}$ mutant (139[+25aa]), which has a short open reading frame before the initiation codon causing reduced protein synthesis (17% of WT) and shows delayed replication kinetics [39], was used as a control in this study.

**Plasmids.** Expression vectors for N-terminally FLAG-tagged PI4KB mutants (GenBank: NM_001198773, UniProt: Q9UBF8-2) were constructed with pTK-Gluc vector (NEW ENGLAND BioLabs) [13]. Expression vectors for N-terminally EGFP-tagged PV 2BC3ABCD polyprotein were constructed with pHEK293 Ultra Expression Vector I (Takara Bio).

**Compounds.** A specific PI4KB inhibitor, T-00127-HEV1, was supplied by Pharmeks (P2001S-271690, purity >99%, determined by liquid chromatography-mass spectrometry [LC-MS]) [8]. An OSBP inhibitor, T-00127-HEV2 [11], was kindly provided from Hirotatsu Kojima (Drug Discovery Initiative, The University of Tokyo) (purity >99%, determined by LC-MS). The 23-(dipyrromethene boron difluoride)-24-norcholesterol (BODIPY-cholesterol) was purchased from Avanti Polar Lipids (810255P).

**Isolation of PV mutant from RD(Δ*PI4KB*) cells.** RD(Δ*PI4KB*) cells ($5 \times 10^3$ cells) were infected with PV1(Sabin) at a multiplicity of infection (MOI) of 50. Cells were incubated at 37°C until all cells exhibited cytopathic effect for 7 days. Collected cell lysates were diluted 100-fold with 10%FCS/DMEM, then used for the next passage. Passage was repeated nine times. A PV mutant clone was isolated by limiting dilution. Protein-coding regions of viral genomes were analyzed as previously described [48].

**Measurement of anti-PV activities of PI4KB/OSBP inhibitors.** RD(WT) cells or

RD(ΔPI4KB) cells ($7 \times 10^3$ cells per well in 20 μL medium) in 384-well plates (catalog no. 781080; Greiner Bio-One) were inoculated with 10 μL of $PV1_{pv}$ (800 infectious units [IU]) and 10 μL of compound solution. Cells were incubated at 37°C for 7 or 16 h. Luciferase activity in the infected cells was measured with the Steady-Glo luciferase assay system (Promega) using a 2030 ARVO X luminometer (PerkinElmer).

**Development of RO in replication-incompetent system.** RD(WT) cells or RD(ΔPI4KB) cells ($6 \times 10^5$ cells/well) were plated into a 96-well glass bottom SensoPlate (Greiner Bio-One, 655896). Cells were transfected with 200 ng of EGFP-2BC3ABCD expression vectors. At 24 h post-transfection, cells were fixed and stained for 2B as a marker of the RO with rabbit anti-2B antibody and goat anti-rabbit IgG antibody conjugated with Alexa Fluor 568 (Thermo Fischer Scientific, A11036). Images were collected at 20× magnification using a BZ-9000 fluorescence microscopy (Keyence). The number of cells with the RO in a wide perinuclear area observed in PV-infected cells (normal-sized RO) or with the RO in a small area observed in RD(ΔPI4KB) cells (small RO) were counted using CellProfiler software [49]. Cells with the normal-sized RO (median typical diameter, 23 pixels) or with the small RO (median typical diameter, 12 pixels) were detected in a typical diameter range of 16 to 40 pixels or 10 to 15 pixels, respectively.

**Flow cytometry.** HEK293 cells ($8.0 \times 10^5$ cells) infected with $PV1_{pv}$ at an MOI of 1 in the absence or presence of T-00127-HEV1 (10 μM). Cells were collected at 7 h p.i. in 0.8 mL of 10%FCS-DMEM, then fixed with 3% paraformaldehyde for 10 min at room

temperature, and permeabilized with 20 μM digitonin in HBS for 5 min. Cells were incubated with anti-2B and PI4P antibodies for 30 min at 37°C. Cells were washed 2 times by 0.5% BSA in HBS, then incubated with secondary antibodies conjugated with Alexa Fluor 647 (for detection of anti-2B antibody) and Alexa Fluor 488 (for detection of anti-PI4P antibody) dyes for 20 min at 37°C. Cells were suspended in 250 μL of HBS. About $5.0 \times 10^4$ cells were measured per sample with a BD FACSCanto™ II Flow Cytometer (BD Biosciences). Data were analyzed using FlowJo software (FLOWJO, LLC). Relative intensity of PI4P signals was determined as below:

$$\text{Relative intensity of PI4P signals} = \left(\frac{\text{PI4P signals in PV1pv} - \text{infected cells}}{\text{PI4P signals in non} - \text{infected cells}}\right)$$

Net amount of produced PI4P was determined as below:

$$\text{Net amount of produced PI4P} = \text{relative intensity of PI4P signals} - 1$$

**Anti-PV activity of IFN.** Human IFN alpha A was purchased from PBL Biomedical Laboratories (11100-1). RD(WT) cells or RD(Δ*PI4KB*) cells were pre-treated with human IFN alpha (final concentration, 1,000 U/mL) for 24 h. IFN response of pre-treated cells was confirmed by up-regulation of OAS1 and STAT1 mRNAs using an IFN Response Watcher qPCR kit (3720, Takara Bio). IFN-treated cells were infected with 800 IU of $PV1_{pv}$. Cells were incubated at 37°C for 16 h, then the luciferase activity in cells was measured.

**Statistical analysis.** Results of experiments are shown as means with standard

deviations. Values of $P<0.05$ by one-tailed *t* test were considered to indicate a significant difference, and were indicated by asterisks (*$P < 0.05$, **$P < 0.01$, ***$P < 0.001$).

**Supporting information**

Figure S1. Evolutionary pathway of PV in RD(Δ*PI4KB*) cells.

Figure S2. Replication kinetics of $PV1_{pv}$ mutants.

Figure S3. Localization of nascent viral RNA and 2B.

Figure S4. Effect of the 3A(G5318A[3A-A70T]) mutation on the RO development.

Figure S5. Specificity of the 3A mutations for the synthetic effect with the 2B mutations.

Figure S6. Effect of the 3A mutations on the processing of viral proteins.

Figure S7. Gating strategy of flow cytometry.

Figure S8. Quantification of PI4P and cholesterol in infected RD(Δ*PI4KB*) cells.

Figure S9. Effects of T-00127-HEV2 on lipid transfer activities of OSBP.

Figure S10. *Trans*-complementation with viral proteins.

Figure S11. Effect of OSBP inhibitors on $PV1_{pv}$ infection.

**Methods:** Methods for Supporting information

**Reference:** Reference for Supporting information

**Author Information**

**Corresponding Author**

*Phone:+81-42-561-0771. Fax:+81-42-561-4729. E-mail: minetaro@nih.go.jp

**ORCID**

Minetaro Arita: 0000-0002-3314-6626

Joëlle Bigay: 0000-0002-7487-3416

**Author contributions**

M.A. conceived the project. M.A. designed the study. J.B. performed lipid transfer assay by OSBP. M.A. performed other assays. M.A. wrote the manuscript. J.B. commented on the manuscript.

**Funding**

This study was in part supported by JSPS KAKENHI Grant Number 16K08822 and Advanced Research & Development Programs for Medical Innovation (AMED-CREST) Grant Number 18gm0910005j0104 from Japan Agency for Medical Research and Development, AMED to M.A.

The funders had no role in study design, data collection and analysis, decision to publish, or preparation of the manuscript.

**Notes**

The authors declare no conflict of interest.

**Acknowledgements**

We are grateful to Junko Wada and Yuzuru Aoi for their excellent technical

assistance, to Hiroyuki Shimizu and Masamichi Muramatsu for their kind support, to Hirotatsu Kojima (Drug Discovery Initiative, The University of Tokyo) for the kind gift of T-00127-HEV2, to Angel Galabov (The Stephan Angeloff Institute of Microbiology, Bulgarian Academy of Sciences, Bulgaria) for the kind supply of MDL-860, to Kazuya Shirato (Department of Virology III, National Institute of Infectious Diseases, Japan) for the kind gift of EMCV, to Atsushi Kato (Division of Quality Assurance, National Institute of Infectious Diseases, Japan) for the kind gift of SeV-luc, and to Tomoichiro Oka (Department of Virology II, National Institute of Infectious Diseases, Japan) for the kind gift of anti-2C antibody. This study was supported in part by JSPS KAKENHI Grant Number 16K08822 and Advanced Research & Development Programs for Medical Innovation (AMED-CREST) Grant Number 18gm0910005j0104 from the Japan Agency for Medical Research and Development, AMED to M.A.

**Abbreviations**

25-HC: 25-hydroxycholesterol

BFA: brefeldin A

EMCV: encephalomyocarditis virus

MOI: multiplicity of infection

OSBP: oxysterol-binding protein

p.i.: post-infection

PI4KB: phosphatidylinositol-4 kinase III beta

PI4P: phosphatidylinositol 4-phosphate

p.t.: post-transfection

PV: poliovirus

$PV1_{pv}$: type 1 PV pseudovirus

RO: replication organelle

**References**


1 Bodian, D. Histopathologic basis of clinical findings in poliomyelitis. *Am. J. Med.* **6**, 563-578. (1949).

2 Couderc, T. *et al.* Molecular pathogenesis of neural lesions induced by poliovirus type 1. *J. Gen. Virol.* **70**, 2907-2918 (1989).

3 Wikel, J. H. *et al.* Synthesis of syn and anti isomers of 6-[[(hydroxyimino)phenyl]methyl]-1-[(1-methylethyl)sulfonyl]-1H-ben zimidaz ol-2-amine. Inhibitors of rhinovirus multiplication. *J. Med. Chem.* **23**, 368-372, doi:10.1021/jm00178a004 (1980).

4 Ishitsuka, H., Ohsawa, C., Ohiwa, T., Umeda, I. & Suhara, Y. Antipicornavirus flavone Ro 09-0179. *Antimicrob. Agents Chemother.* **22**, 611-616, doi:10.1128/AAC.22.4.611 (1982).

5 Galabov, A. S., Nikolaeva, L. & Philipov, S. Aporphinoid alkaloid glaucinone: a selective inhibitor of poliovirus replication. *Antiviral. Res.* **26**, A347 (1995).

6 Arita, M., Wakita, T. & Shimizu, H. Characterization of pharmacologically active compounds that inhibit poliovirus and enterovirus 71 infectivity. *J. Gen. Virol.* **89**, 2518-2530, doi:10.1099/vir.0.2008/002915-0 (2008).

7 De Palma, A. M. *et al.* Mutations in the non-structural protein 3A confer resistance to the novel enterovirus replication inhibitor TTP-8307. *Antimicrob. Agents Chemother.* **53**, 1850-1857, doi:10.1128/AAC.00934-08 (2009).

8 Arita, M. *et al.* Phosphatidylinositol 4-kinase III beta is a target of enviroxime-like compounds for antipoliovirus activity. *J. Virol.* **85**, 2364-2372, doi:10.1128/JVI.02249-10 (2011).

9 Delang, L., Paeshuyse, J. & Neyts, J. The role of phosphatidylinositol 4-kinases and phosphatidylinositol 4-phosphate during viral replication. *Biochem. Pharmacol.* **84**, 1400-1408, doi:10.1016/j.bcp.2012.07.034 (2012).

10 MacLeod, A. M. *et al.* Identification of a series of compounds with potent antiviral activity for the treatment of enterovirus infections. *ACS Med. Chem. Lett.* **4**, 585-589, doi:10.1021/ml400095m (2013).

11 Arita, M. *et al.* Oxysterol-binding protein family I is the target of minor enviroxime-like compounds. *J. Virol.* **87**, 4252-4260, doi:10.1128/JVI.03546-12 (2013).

12 Strating, J. R. *et al.* Itraconazole Inhibits Enterovirus Replication by Targeting the Oxysterol-Binding Protein. *Cell Rep.*, doi:10.1016/j.celrep.2014.12.054 (2015).

13 Arita, M., Dobrikov, G., Purstinger, G. & Galabov, A. S. Allosteric Regulation of Phosphatidylinositol 4-Kinase III Beta by an Antipicornavirus Compound MDL-860. *ACS Infect. Dis.* **3**, 585-594, doi:10.1021/acsinfecdis.7b00053 (2017).

14 Hsu, N. Y. *et al.* Viral reorganization of the secretory pathway generates distinct organelles for RNA replication. *Cell* **141**, 799-811, doi:10.1016/j.cell.2010.03.050 (2010).
15 Knight, Z. A. *et al.* A pharmacological map of the PI3-K family defines a role for p110alpha in insulin signaling. *Cell* **125**, 733-747, doi:10.1016/j.cell.2006.03.035 (2006).
16 Balla, T. Phosphoinositides: tiny lipids with giant impact on cell regulation. *Physiol. Rev.* **93**, 1019-1137, doi:10.1152/physrev.00028.2012 (2013).
17 Albulescu, L. *et al.* Uncovering oxysterol-binding protein (OSBP) as a target of the anti-enteroviral compound TTP-8307. *Antiviral Res.* **140**, 37-44, doi:10.1016/j.antiviral.2017.01.008 (2017).
18 Mesmin, B. *et al.* A Four-Step Cycle Driven by PI(4)P Hydrolysis Directs Sterol/PI(4)P Exchange by the ER-Golgi Tether OSBP. *Cell* **155**, 830-843, doi:10.1016/j.cell.2013.09.056 (2013).
19 Olkkonen, V. M. & Li, S. Oxysterol-binding proteins: sterol and phosphoinositide sensors coordinating transport, signaling and metabolism. *Prog. Lipid Res.* **52**, 529-538, doi:10.1016/j.plipres.2013.06.004 (2013).
20 Ridgway, N. D. & Zhao, K. Cholesterol transfer at endosomal-organelle membrane contact sites. *Curr. Opin. Lipidol.* **29**, 212-217, doi:10.1097/MOL.0000000000000506 (2018).
21 Antonny, B., Bigay, J. & Mesmin, B. The Oxysterol-Binding Protein Cycle: Burning Off PI(4)P to Transport Cholesterol. *Annu. Rev. Biochem.* **87**, 809-837, doi:10.1146/annurev-biochem-061516-044924 (2018).
22 Heinz, B. A. & Vance, L. M. The antiviral compound enviroxime targets the 3A coding region of rhinovirus and poliovirus. *J. Virol.* **69**, 4189-4197 (1995).
23 Rodriguez, P. L. & Carrasco, L. Gliotoxin: inhibitor of poliovirus RNA synthesis that blocks the viral RNA polymerase 3Dpol. *J. Virol.* **66**, 1971-1976 (1992).
24 Arita, M. Phosphatidylinositol-4 kinase III beta and oxysterol-binding protein accumulate unesterified cholesterol on poliovirus-induced membrane structure. *Microbiol. Immunol.* **58**, 239-256, doi:10.1111/1348-0421.12144 (2014).
25 Arita, M. Mechanism of Poliovirus Resistance to Host Phosphatidylinositol-4 Kinase III ß Inhibitor. *ACS Infectious Diseases* **2**, 140-148, doi:10.1021/acsinfecdis.5b00122 (2016).
26 Melia, C. E. *et al.* Escaping Host Factor PI4KB Inhibition: Enterovirus Genomic RNA Replication in the Absence of Replication Organelles. *Cell reports* **21**, 587-599, doi:10.1016/j.celrep.2017.09.068 (2017).
27 Lyoo, H., Dorobantu, C. M., van der Schaar, H. M. & van Kuppeveld, F.

J. M. Modulation of proteolytic polyprotein processing by coxsackievirus mutants resistant to inhibitors targeting phosphatidylinositol-4-kinase IIIbeta or oxysterol binding protein. *Antiviral Res* **147**, 86-90, doi:10.1016/j.antiviral.2017.10.006 (2017).

28 Banerjee, S. *et al.* Hijacking of multiple phospholipid biosynthetic pathways and induction of membrane biogenesis by a picornaviral 3CD protein. *PLoS Pathog.* **14**, e1007086, doi:10.1371/journal.ppat.1007086 (2018).

29 Ishikawa-Sasaki, K., Nagashima, S., Taniguchi, K. & Sasaki, J. Model of OSBP-Mediated Cholesterol Supply to Aichi Virus RNA Replication Sites Involving Protein-Protein Interactions among Viral Proteins, ACBD3, OSBP, VAP-A/B, and SAC1. *J. Virol.* **92**, doi:10.1128/JVI.01952-17 (2018).

30 Sagan, S. M. *et al.* The influence of cholesterol and lipid metabolism on host cell structure and hepatitis C virus replication. *Biochem. Cell Biol.* **84**, 67-79, doi:10.1139/o05-149 (2006).

31 Bianco, A. *et al.* Metabolism of phosphatidylinositol 4-kinase IIIalpha-dependent PI4P Is subverted by HCV and is targeted by a 4-anilino quinazoline with antiviral activity. *PLoS Pathog.* **8**, e1002576, doi:10.1371/journal.ppat.1002576 (2012).

32 Wang, H. *et al.* Oxysterol-binding protein is a phosphatidylinositol 4-kinase effector required for HCV replication membrane integrity and cholesterol trafficking. *Gastroenterology* **146**, 1373-1385 e1371-1311, doi:10.1053/j.gastro.2014.02.002 (2014).

33 Esser-Nobis, K., Harak, C., Schult, P., Kusov, Y. & Lohmann, V. Novel perspectives for hepatitis A virus therapy revealed by comparative analysis of hepatitis C virus and hepatitis A virus RNA replication. *Hepatology* **62**, 397-408, doi:10.1002/hep.27847 (2015).

34 Harak, C. *et al.* Tuning a cellular lipid kinase activity adapts hepatitis C virus to replication in cell culture. *Nat. Microbiol.* **2**, 16247, doi:10.1038/nmicrobiol.2016.247 (2016).

35 Wang, H. & Tai, A. W. Continuous de novo generation of spatially segregated hepatitis C virus replication organelles revealed by pulse-chase imaging. *J. Hepatol.* **66**, 55-66, doi:10.1016/j.jhep.2016.08.018 (2017).

36 Dorobantu, C. M. *et al.* Modulation of the Host Lipid Landscape to Promote RNA Virus Replication: The Picornavirus Encephalomyocarditis Virus Converges on the Pathway Used by Hepatitis C Virus. *PLoS Pathog.* **11**, e1005185, doi:10.1371/journal.ppat.1005185 (2015).

37 van der Schaar, H. M. *et al.* A novel, broad-spectrum inhibitor of enterovirus replication that targets host cell factor phosphatidylinositol 4-kinase IIIbeta. *Antimicrob. Agents Chemother.* **57**, 4971-4981, doi:10.1128/AAC.01175-13 (2013).

38 Berryman, S., Moffat, K., Harak, C., Lohmann, V. & Jackson, T. Foot-and-mouth disease virus replicates independently of phosphatidylinositol 4-phosphate and type III phosphatidylinositol 4-kinases. *J. Gen. Virol.* **97**, 1841-1852, doi:10.1099/jgv.0.000485 (2016).

39 Arita, M., Shimizu, H. & Miyamura, T. Characterization of in vitro and in vivo phenotypes of poliovirus type 1 mutants with reduced viral protein synthesis activity. *J. Gen. Virol.* **85**, 1933-1944 (2004).

40 Heinz, B. A. & Vance, L. M. Sequence determinants of 3A-mediated resistance to enviroxime in rhinoviruses and enteroviruses. *J. Virol.* **70**, 4854-4857 (1996).

41 Xiao, X. *et al.* Enterovirus 3A facilitates viral replication by promoting PI4KB-ACBD3 interaction. *J. Virol.* **91**, e00791-00717, doi:10.1128/JVI.00791-17 (2017).

42 Belov, G. A. *et al.* Complex dynamic development of poliovirus membranous replication complexes. *J. Virol.* **86**, 302-312, doi:10.1128/JVI.05937-11 (2012).

43 Mesmin, B. *et al.* Sterol transfer, PI4P consumption, and control of membrane lipid order by endogenous OSBP. *EMBO J* **36**, 3156-3174, doi:10.15252/embj.201796687 (2017).

44 Ida-Hosonuma, M. *et al.* The alpha/beta interferon response controls tissue tropism and pathogenicity of poliovirus. *J. Virol.* **79**, 4460-4459 (2005).

45 Xiao, Y. *et al.* Poliovirus intrahost evolution is required to overcome tissue-specific innate immune responses. *Nat. Commun.* **8**, 375, doi:10.1038/s41467-017-00354-5 (2017).

46 Viktorova, E. G., Nchoutmboube, J. A., Ford-Siltz, L. A., Iverson, E. & Belov, G. A. Phospholipid synthesis fueled by lipid droplets drives the structural development of poliovirus replication organelles. *PLoS Pathog* **14**, e1007280, doi:10.1371/journal.ppat.1007280 (2018).

47 Sanjana, N. E., Shalem, O. & Zhang, F. Improved vectors and genome-wide libraries for CRISPR screening. *Nat Methods* **11**, 783-784, doi:10.1038/nmeth.3047 (2014).

48 Arita, M. *et al.* A Sabin 3-derived poliovirus recombinant contained a sequence homologous with indigenous human enterovirus species C in the viral polymerase coding region. *J. Virol.* **79**, 12650-12657 (2005).

49 Kamentsky, L. *et al.* Improved structure, function and compatibility for CellProfiler: modular high-throughput image analysis software. *Bioinformatics* **27**, 1179-1180, doi:10.1093/bioinformatics/btr095 (2011).

**Table 1. Virus titers in RD(WT) and RD(ΔPI4KB) cells**

| | $CCID_{50}$ (in 100 µL) | | | |
|---|---|---|---|---|
| **Virus** | **RD(WT)** | **RD(Δ*PI4KB*)** | **Number of copies of viral genome (in 100 µL)** | **Number of copies of viral genome / $CCID_{50}$ in RD(WT) cells** |
| PV1(Sabin) | $10^{8.5(0.5)}$ | $10^{2.8(0.0)}$ | $4.0(0.29) \times 10^{10}$ | 110(8.1) |
| PV1(Δ*PI4KB* resistant) | $10^{7.7(0.2)}$ | $10^{7.7(0.2)}$ | $6.2(0.47) \times 10^{10}$ | 1,200(93) |
| EMCV | $10^{7.7(0.0)}$ | $10^{7.5(0.3)}$ | n.d. | n.d. |

Standard deviation is shown in parentheses. n.d.; not determined. $n = 2$.

**Figure 1. Generation of *PI4KB*-knockout cell line highly resistant to PV infection.**
**(A)** Nt sequences of *PI4KB* alleles in RD(WT) and RD(Δ*PI4KB*) cells around the target site of CIRSPR/Cas9-mediated gene edition (colored by blue). Nt number of mRNA of *PI4KB* transcript variant 2 (GenBank:NM_001198773) and encoded aa are shown.
**(B)** Western blot analysis of PI4KB in RD(WT) and RD(Δ*PI4KB*) cells.
**(C)** Rescue of $PV1_{pv}$(WT) infection by ectopic expression of PI4KB in RD(Δ*PI4KB*) cells. $PV1_{pv}$(WT) infection in RD(Δ*PI4KB*) cells expressing N-FLAG-PI4KB(WT, C646S, or D656A) in the presence of MDL-860. $PV1_{pv}$ infection in RD(Δ*PI4KB*) cells expressing N-FLAG-PI4KB(WT) in the absence of MDL-860 was taken as 100%.
**(D)** Infectivity of $PV1_{pv}$ and Sendaivirus in RD(Δ*PI4KB*). RD(WT) and RD(Δ*PI4KB*) cells were infected with $PV1_{pv}$ or SeV-luc at indicated MOI, then luciferase activity was measured at 7 or 24 h p.i., respectively. $PV1_{pv}$(WT) infection at an MOI of 27 or SeVluc infection at an MOI of 2.9 in RD(WT) cells are taken as 100%. Relative infectivity in RD(Δ*PI4KB*) cells is shown. $n = 3$.

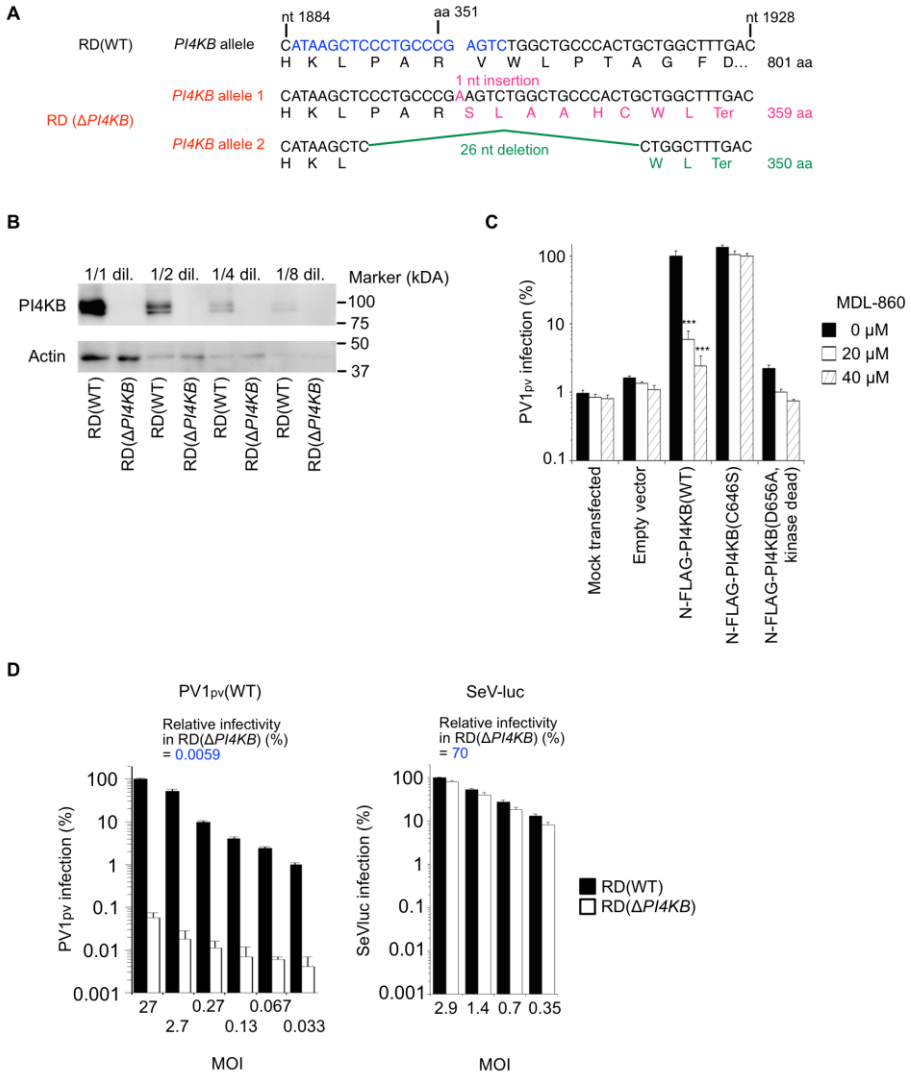

**Figure 2. Isolation of PV mutant from RD(Δ*PI4KB*) cells.**
**(A)** Schematic view of PV1(Δ*PI4KB* resistant) genome.
**(B)** Infectivity of $PV1_{pv}$ mutants in RD(Δ*PI4KB*) cells. Filled diamonds represent nt mutation derived from PV1(Δ*PI4KB* resistant), and open diamonds represent nt of WT. Relative and normalized infectivity of $PV1_{pv}$ mutants in RD(Δ*PI4KB*) cells are shown. In relative infectivity in RD(Δ*PI4KB*) cells, $PV1_{pv}$ infection at 7 or 16 h p.i. in RD(WT) cells are taken as 100%. In normalized infectivity in RD(Δ*PI4KB*) cells, relative infectivity of $PV1_{pv}$(WT) is taken as 1. Standard deviation is shown in parentheses. n.s., not significant. $n = 3$.

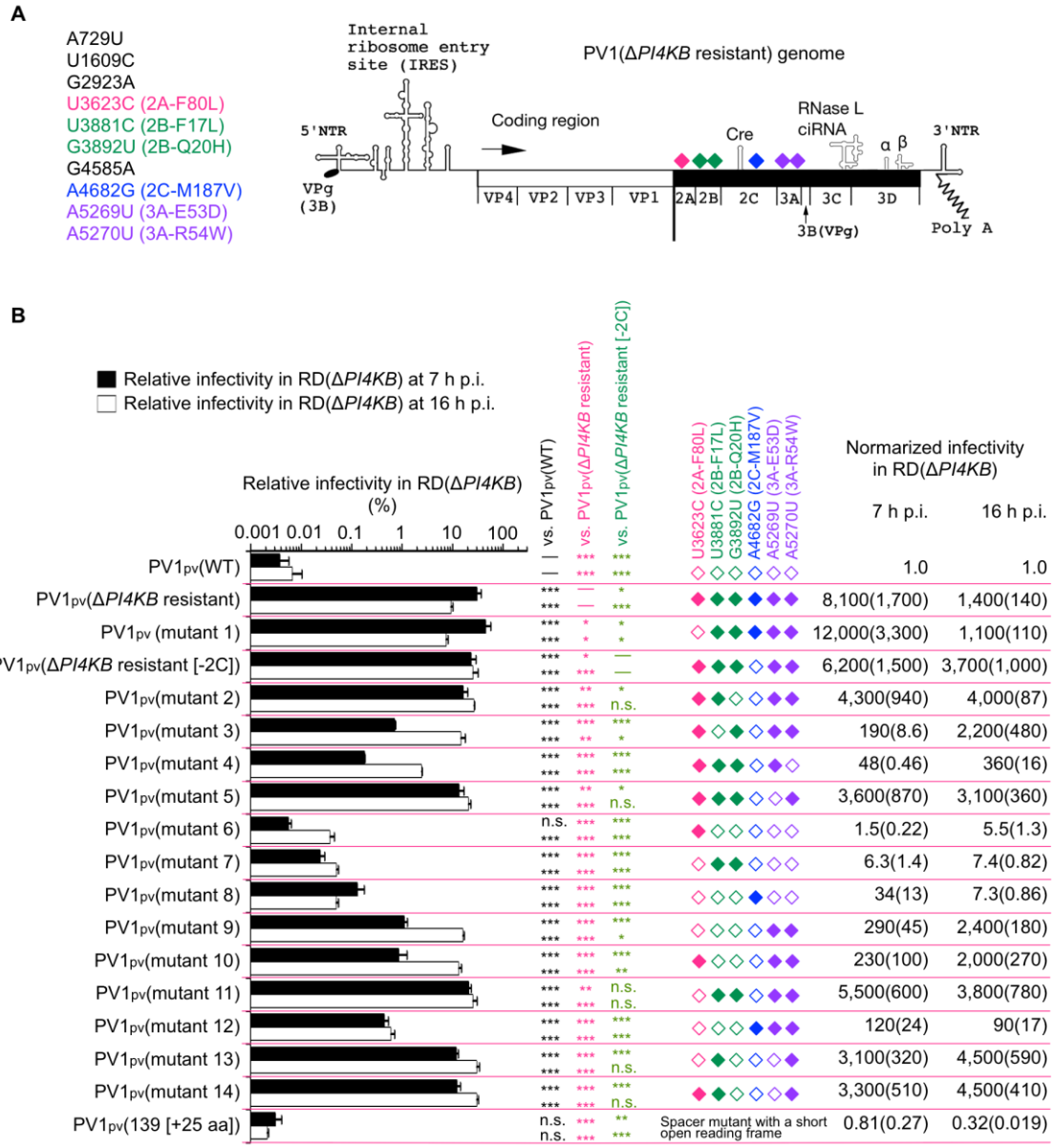

**Figure 3. Effect of the 3A and 2B mutations on the RO development.**
N-terminally EGFP-fused PV polyprotein (EGFP-2BC3ABCD) with indicated mutations were overexpressed in RD(WT) and RD(Δ*PI4KB*) cells. Localization of 2B was analyzed as a marker of RO. Populations of cells with normal-sized or small RO are shown. n.s., not significant (vs. EGFP-2BC3ABCD[WT]).

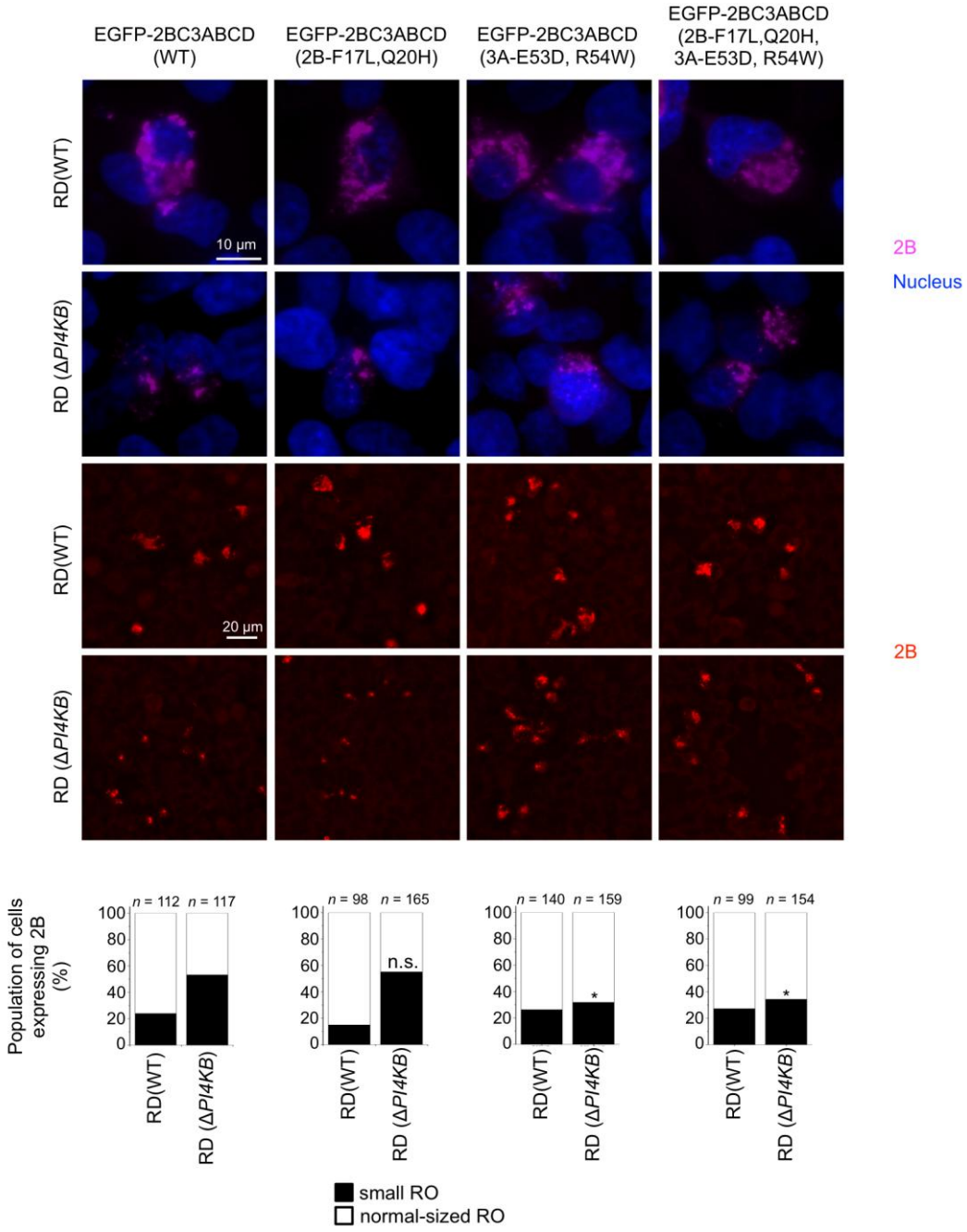

**Figure 4. Effect of 2B mutations on PV replication.**
Luciferase signals in a single $PV1_{pv}$-infected cell at 7 or 16 h p.i. Filled diamonds of $PV1_{pv}$ represent nt mutation derived from PV1(Δ*PI4KB* resistant), and open diamonds represent nt of WT. Relative light units (RLU) per infected cells are shown. *n* = 3. n.d.; not detectable.

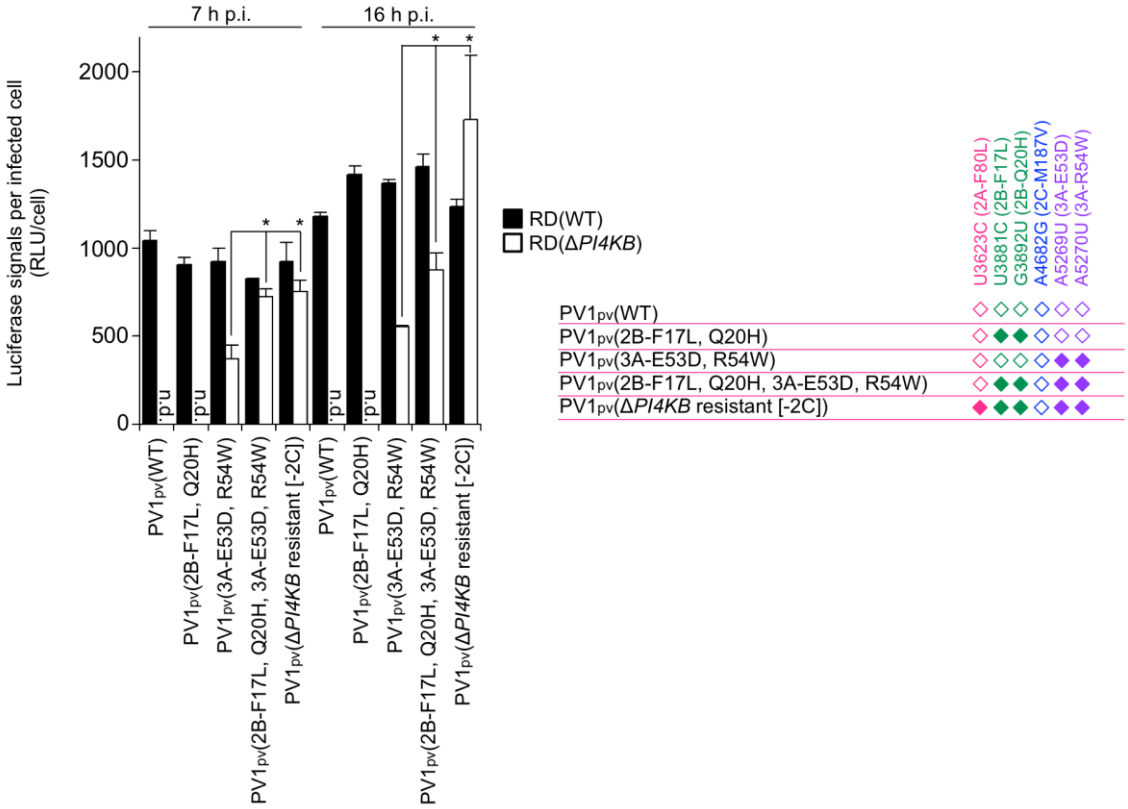

**Figure 5. Quantification of PI4P and cholesterol in infected RD(WT) cells.**
Left panels: Localization of 2B, cholesterol, PI4P in RD(WT) cells infected with $PV1_{pv}$(WT) at 7 h p.i. or with $PV1_{pv}$(Δ*PI4KB* resistant [-2C]) at 7 or 16 h p.i. at an MOI of 2.5 in the absence or presence of T-00127-HEV1 (10 μM). Cyan, filipin III (staining of unesterified cholesterol); green, PI4P; magenta, 2B.
Right panels: Flow cytometry analysis of RD(WT) cells infected with $PV1_{pv}$(WT) or $PV1_{pv}$(Δ*PI4KB* resistant [-2C]) at an MOI of 1.0 in the absence or presence of T-00127-HEV1 (10 μM) at indicated time with anti-2B and anti-PI4P antibodies. Ratios of geometric means of PI4P signals in the $PV1_{pv}$-infected cells to non-infected cells are determined with standard deviation (in parenthesis) in the right graphs. $n$ = 3. n.d.; not detectable.

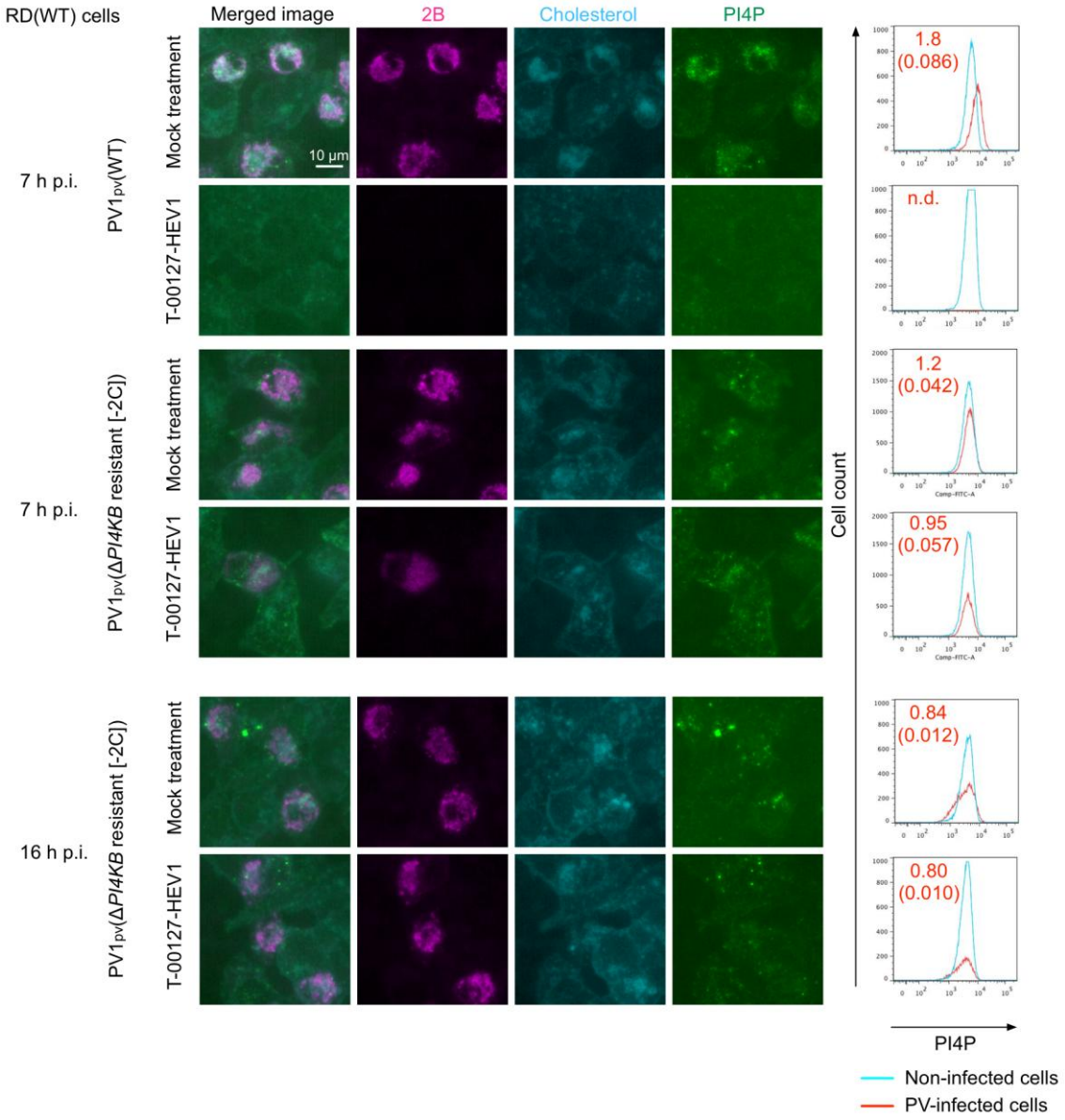

**Figure 6. Quantification of PI4P in infected RD(WT) cells.**
**(A)** Flow cytometry analysis of RD(WT) cells infected with $PV1_{pv}$s at an MOI of 0.5 at 7 h p.i. with anti-2B and anti-PI4P antibodies. Ratios of geometric means of PI4P signals in $PV1_{pv}$-infected cells to non-infected cells are determined with standard deviation (in parenthesis).
**(B)** Effect of the mutations of PV1(Δ*PI4KB* resistant) on the relative PI4P level of infected cells. n.s., not significant. $n = 3$.

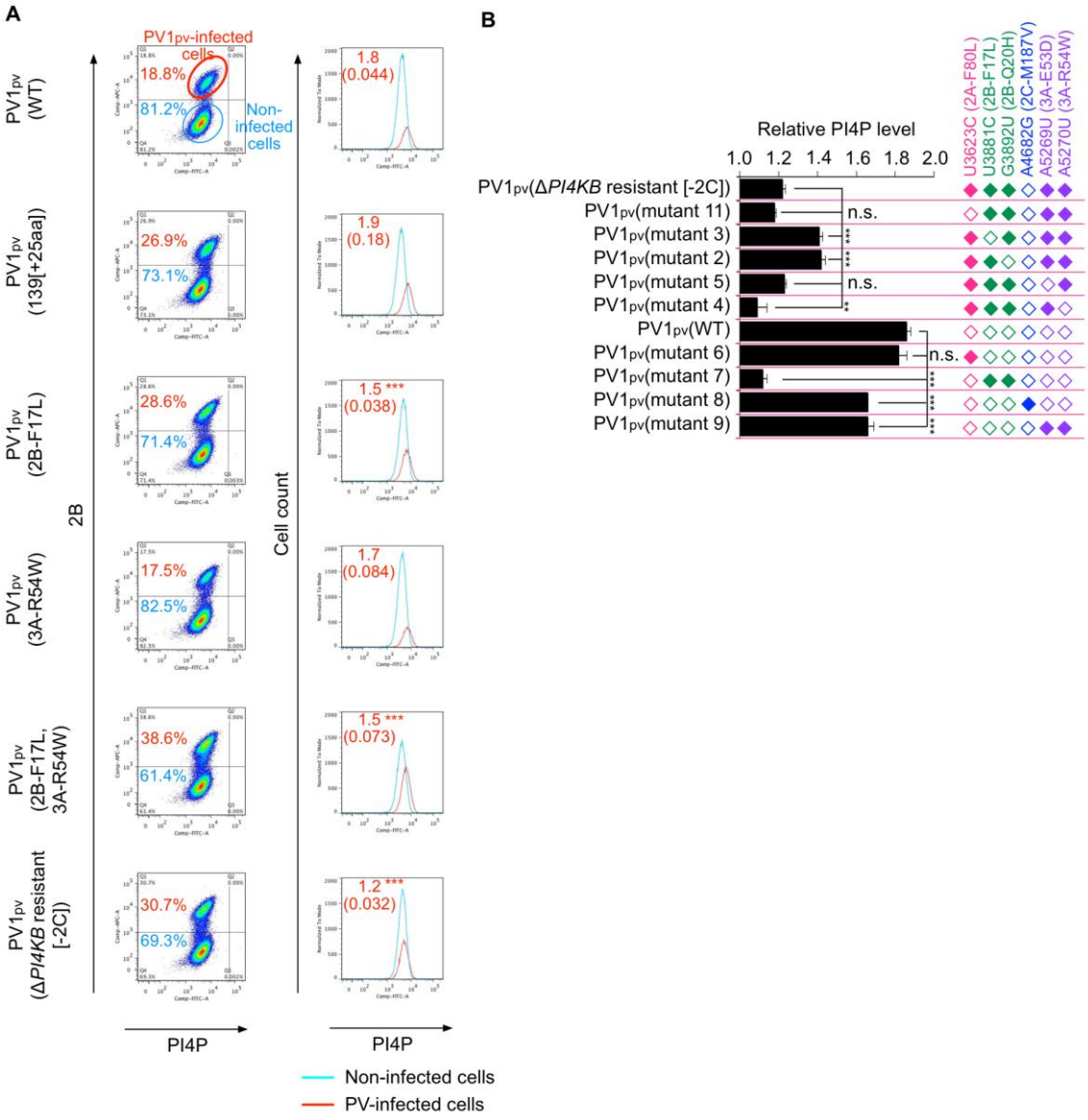

**Figure 7. Cross resistance of PV1$_{pv}$(Δ*PI4KB* resistant) to PI4KB/OSBP inhibitors.** Inhibitory effects of PI4KB/OSBP inhibitors on the infection of PV1$_{pv}$ mutants in **(A)** RD(WT) cells or in **(B)** RD(Δ*PI4KB*) cells. PV1$_{pv}$ infection in the absence of compounds is taken as 100%. Filled diamonds of PV1$_{pv}$ represent nt mutation derived from PV1(Δ*PI4KB* resistant), and open diamonds represent nt of WT. *n* = 3.

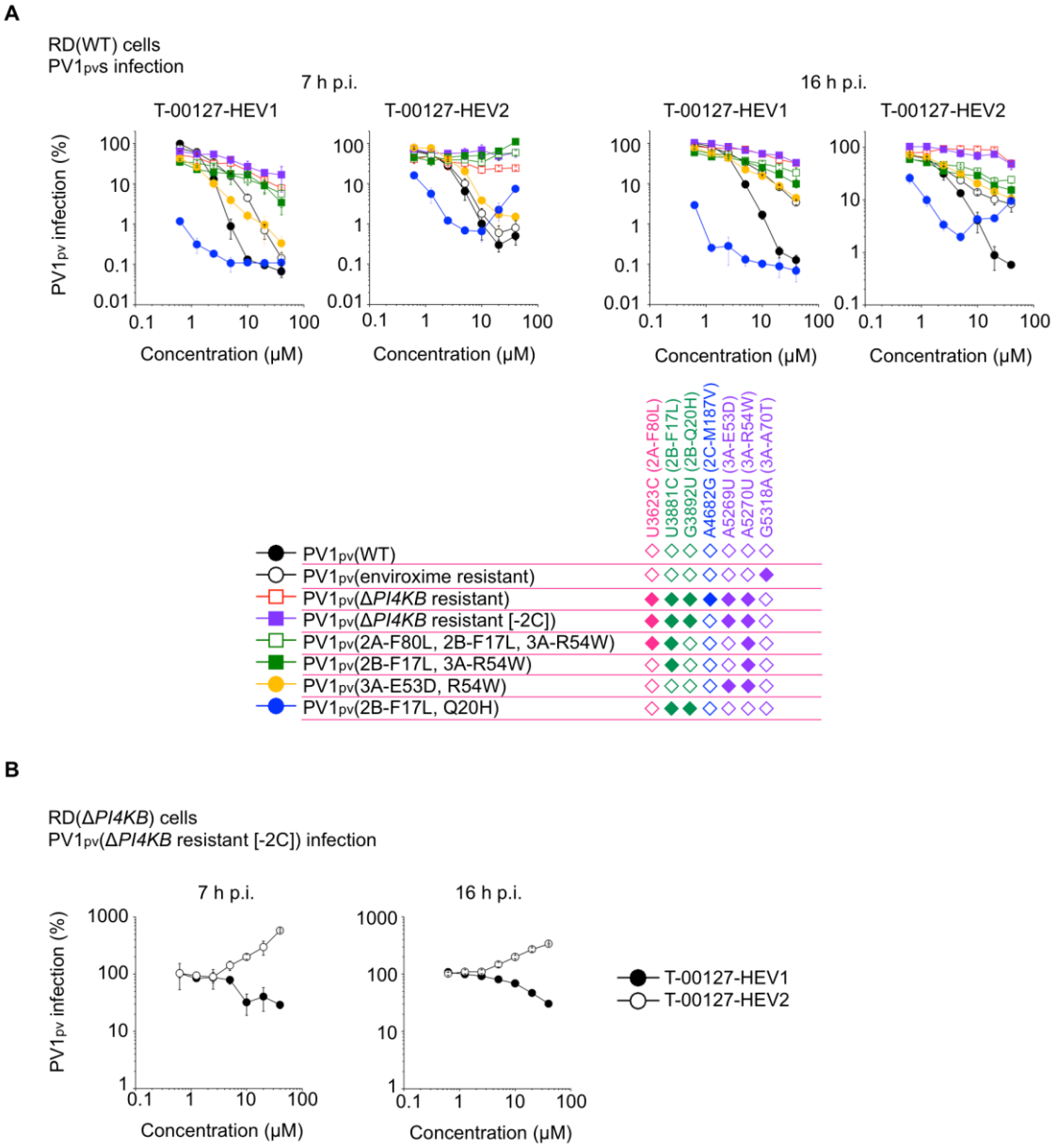

**Figure 8. Effect of type I IFN on $PV1_{pv}$(Δ*PI4KB* resistant) infection.**
RD(WT) cells or in RD(Δ*PI4KB*) cells were pre-treated with human interferon alpha (1,000 U/mL) for 24 h, then infected with $PV1_{pv}$. $PV1_{pv}$ infection in the absence of interferon is taken as 100%. Filled diamonds of $PV1_{pv}$ represent nt mutation derived from PV1(Δ*PI4KB* resistant), and open diamonds represent nt of WT. n.d.; not detectable. n.s., not significant. $n = 3$.